



Fast Simulation for the Super Charm-Tau Factory Detector

Alexander Barnyakov^{1,3} · Maria Belozyorova² · Victor Bobrovnikov^{1,2} · Sergey Kononov^{1,2} · Dmitriy Kyshtymov^{1,2} · Dmitriy Maksimov^{1,2} · Georgiy Razuvaev^{1,2} · Andrey Sukharev^{1,2} · Korneliy Todyshev^{1,2} · Vitaliy Vorobyev¹ · Anastasiia Zhadan^{1,2} · Daniil Zhadan^{1,2}

Received: 22 November 2022 / Accepted: 7 December 2023
© The Author(s) 2023

Abstract

The Super Charm-Tau factory (high luminosity electron-positron collider with 3–7 GeV center of mass energy range) experiment project is under development by the consortium of Russian scientific and education organizations. The article describes the present status of the Super Charm-Tau detector fast simulation and the algorithms on which it is based, example usage and demonstration of fast simulation results.

Keywords Super Charm-Tau factory · Fast simulation · Parametric simulation

Introduction

The Super Charm-Tau (SCT) factory is an electron-positron collider project planned to be built under Budker INP leadership in Russia, with peak luminosity of $10^{35} \text{ cm}^{-2} \text{ s}^{-1}$ and center of mass energy ranging from 3 to 7 GeV. The total integrated luminosity expected to be acquired during the experiment operation is approximately 10 ab^{-1} [1–3]. One of the key features of the project is a high level (80–90%) electron beam longitudinal polarization at the interaction point, which will be equipped with a universal particle detector. The proposed combination of collider and high performance detector would allow a series of precise experiments and tests of the Standard Model (SM), particularly to make a systematic study of hadrons consisting of u , d , s and c quarks, including exotic states, and \mathcal{CP} -violation in systems of charm hadrons or τ leptons, as well as charge lepton

flavour violation. For more details the reader is referred to [1] and [2].

Super Charm-Tau Detector

The SCT detector is envisaged to be an almost full solid angle detector with 1.5 T axial magnetic field provided by a superconducting magnet, consisting of tracking system, charged particles identification system, electromagnetic calorimeter, and muon system, as shown in the Fig. 1.

At this stage of the project, the detector construction is not finalized yet. Several options are under consideration for various subsystems, enumerated below.

The tracking system encloses the beams collision point and consists of inner and outer trackers. The inner tracker options under consideration are a silicon strip tracker, a cylindrical microgaseous detector, and a time-projection chamber. The main tracker is represented by a drift chamber (DC). Two options are considered: a classical DC with axial and stereo layers and full stereo low material budget DC, both being able to provide dE/dx measurement and cluster counting. The main option for the particle identification (PID) is focusing aerogel ring imaging Cherenkov (FARICH) system. It is surrounded by pure CsI crystal electromagnetic calorimeter. All these systems are placed inside a superconducting solenoid magnet. Iron plates of the magnet yoke serve as absorbers for the multi-layered muon system based on plastic scintillators.

The initial article corresponding author Georgiy Razuvaev died December 27, 2022 in a car accident after the article was submitted.

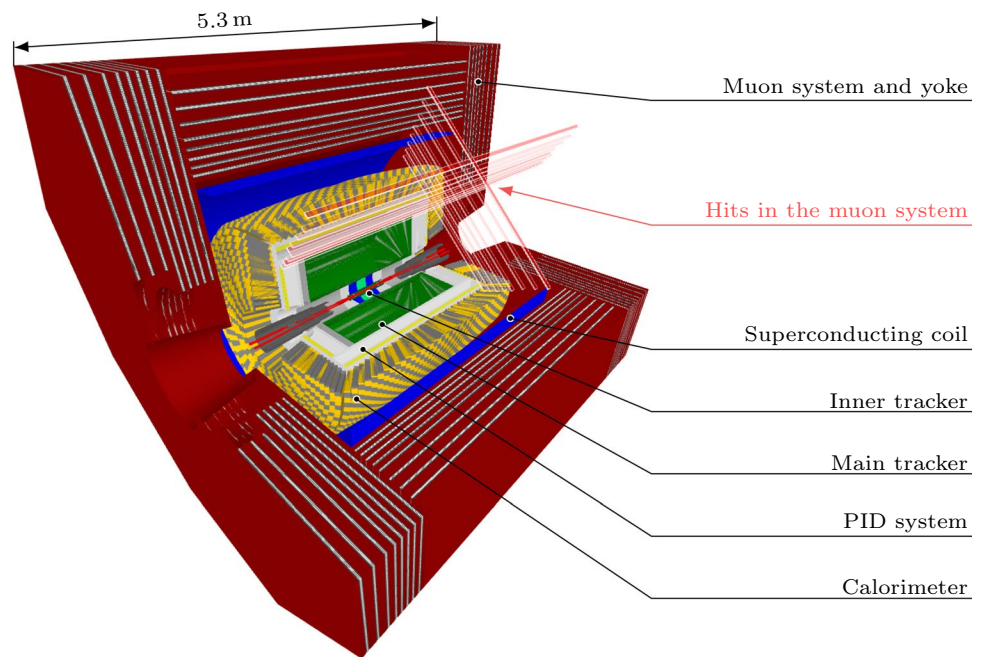
✉ Andrey Sukharev
A.M.Suharev@inp.nsk.su

¹ Budker Institute of Nuclear Physics, 11, Akademika Lavrentieva Prospect, Novosibirsk 630090, Russia

² Novosibirsk State University, 1, Pirogova Street, Novosibirsk 630090, Russia

³ Novosibirsk State Technical University, 20, Karl Marks Prospect, Novosibirsk 630073, Russia

Fig. 1 The SCT detector cut-off view. Muon system hits (see subsect. "Muon System") are shown in the cut out area



Offline Software

The SCT experiment requires a complete stack of relevant software which would provide event generation, parametric and full detector simulation, event digitization and reconstruction algorithms, event data model (EDM), high-level data analysis tools and tests to enable complete analyses. Such a set is usually referred to as a framework. A well-defined and stable computing environment is essential for the framework development and reliable operation.

The SCT detector software framework Aurora [4, 5] is generally inspired by ATLAS Athena [6]. It is based on the de-facto high energy physics (HEP) standard Gaudi [7] and covers all aspects of interaction of different software components at runtime, including configuration, data exchange and job running. The framework components are inherited from Gaudi. These are:

- an Algorithm. It takes input data, manipulates it and produces new output data. This component contains main logic of the program. Usually an algorithm delegates certain aspects of its work to Tools.
- a Tool. Tools are classes that help other components do their job.
- a Service. This component is initialized once and then is used by several Algorithms or Tools. Examples of services are a messaging service, random number generation service, job option service.

The framework components are implemented with C++, while Python is used for configuration and steering scripts. Aurora is structured in packages, each package being responsible for a certain scope, for instance, a package for a subsystem geometry description or event reconstruction. A package contains whatever set of Algorithms/Tools/Services necessary for its tasks.

The data flow in the processing chain is conventional. Events are generated by the generator chosen as most appropriate to the studies, then injected into the simulation, yielding energy deposits in the relevant detector subsystems. The deposits are processed with digitization modules, their output data format being exactly the same as it would be for the real detector hardware. Thus the reconstruction could operate with either simulated or real, in the future, data. Reconstructed events are analysed using corresponding high-level tools. At each stage of this chain the intermediate data could be routed directly from one module to another, or stored and read back later.

The SCT detector event data model is implemented as C++ plain-old-data (POD) objects. The EDM objects are defined in a single yaml [8] file. The PODIO [9] package is used to generate actual C++ classes and provides a serialization mechanisms to store/retrieve data from/to ROOT [10] files. The EDM is not finalized yet, as the software development process often requires introduction of new and adjustment of existing data types.

Simulation: Full, Parametric and Fast

The detector simulation is one of the primary key elements to fulfil the experimental physical program starting from the detector design and finishing with analysis. The simulation should address following tasks:

- Evaluation of detector response to signal and background primary events.
- Establishment of event selection criteria.
- Estimate the expected accuracy of physical results.
- Optimization of detector subsystems, setting the performance requirements.

It should also provide sensible data input to development, debugging and testing other parts of the software like event reconstruction and analysis tools.

The level of detail of the simulation can be either parametric, fast or full, with combinations of these basic types possible.

Full simulation aims to reproduce the detector response very similar to the experimental one. Such a simulation is usually based on detailed description of detector materials, on propagation of particles through the experimental apparatus, and on physics processes that occurs while they do so, for example electromagnetic interactions and particle decays. Aurora utilizes Geant4 toolkit [11–13] for this task. Unlike other kinds of simulation, the full simulation output should be digitized and reconstructed before analysis.

Parametric simulation relies on analytic functions to convert primary generated particle characteristics to reconstructed ones. This kind of simulation does not depend on particular detector subsystem realization, generally dropping the geometry, amount of materials, and hits overlaying. The `SimpleSctParSim` package of parametric simulation has been developed within the Aurora project.

There are several parametric simulation packages available for experiments at high energies ($\sqrt{s} \geq 100$ GeV), for instance, PAPAS (The Parametrized Particle Simulation) [14] is used for simulation of e^+e^- colliders, while Delphes [15] designed for hadron beams collision events. The energies below 10 GeV could be studied with the Chinese Super Tau Charm Factory project fast simulation [16].

Fast simulation is utilized for specific subsystem cases, and still mostly uses analytic functions to get detector response. However, the complexity of such functions increases compared to the parametric simulation case, accounting for the detector geometry and time of particle propagation, yet not directly describing interactions with matter.

The fast simulation packages listed in Sect. "Fast Simulation Software Structure" are developed within the Aurora

framework and are aimed to be used for preliminary analyses and various detector subsystems effectiveness evaluation.

Fast Simulation Software Structure

Following the Aurora architecture and the principle of separation of concerns the SCT fast simulation consists of four packages:

- `SctParSimAlg`—the main algorithm.
- `SctParSimCpp`—this package contains helper classes, in particular to work with geometry.
- `SctParSimTools`—this package is comprised of detector subsystem implementations. At the moment, drift chamber, FARICH PID system, calorimeter and muon system have been implemented.
- `SctParSimInterfaces`—this package contains subsystems interfaces for the tools from `SctParSimTools`.

The `SctParSimAlg` package consists of a single class with the same name. For each particle from the input collection, it calls the detector subsystems tools depending on if the particle charged or not, then gathers all the responses into output collections (see Fig. 2).

`SctParSimAlg` is accompanied by examples, which show the package operation within the Aurora framework, namely reading primary generated data and storing results, interaction with primary particles generators and physics analysis tools.

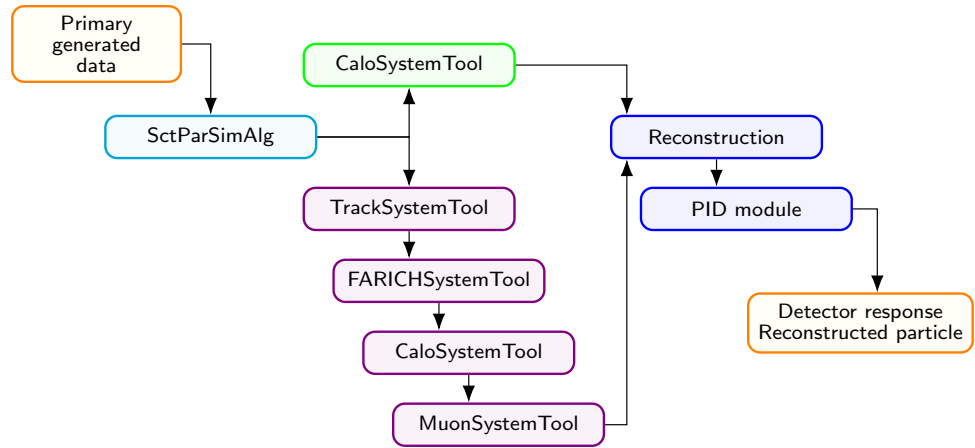
The detector subsystems are included in the `SctParSimTools` package. Each detector subsystem is described as either a single right circular hollow cylinder or multiple cylinders. For example, the drift chamber is associated with a single tube, while the calorimeter has central part and two endcaps.

The main algorithm parameters and the detector subsystems involved are set through the algorithm properties. This allows user to configure the parameters from the script that runs the simulation.

The package `SctParSimCpp` contains two classes: `SctHelix` to describe charged particles tracks with helices (due to detector axial magnetic field) and `SctLine`—neutrals with straight lines. Besides these two classes, the `Crosser` namespace is defined within the package. A set of functions to calculate geometric intersections of tracks with cylinders and tubes is provided in this namespace.

To run the fast simulation one should use a Python script, where the `SctParSim` instance is created, tuned, and passed to the Aurora top algorithm for execution. `SctParSim` algorithms and tools properties can be accessed within

Fig. 2 Fast simulation scheme. Primary data is routed to the simulation using Aurora mechanisms either from a file or directly from a generator



the script as attributes of a Python class. A script example is presented in appendix A.

Implemented Subsystems and Their Parametrizations

The fast simulation implements the DC-based tracker, FARICH, pCsI calorimeter and muon systems. Their parametrizations are described below.

Tracker

Due to the availability of the full geometric description [17], the classical DC tracker is implemented within the fast simulation, still allowing to adjust some parameters to be able to study another DC option too.

Inner tracker options are not studied well enough to provide an adequate parametrization. Hence, the whole tracker is represented only as a drift chamber. The DC inner radius is reduced to overlay the inner tracker space and recover sensitivity to soft tracks.

The DC model is based on wire structures reproducing 10 superlayers of 4 hexagonal cell layers each, where four superlayers are axial and the other six are stereo. Layers are described by cylinders without cell structure. The inner tracker is emulated with additional 4 stereo and 8 axial layers.

The transverse momentum resolution is expressed as

$$\sigma_{\perp} = p_{\perp} \sqrt{(ap_{\perp})^2 + b^2}, \tag{1}$$

where p_{\perp} is the particle transverse momentum (all momenta in this subsection equations are in GeV / c), a and b —resolution coefficients defined with the help of stand-alone simulation [17] as

$$a = a_0 \frac{L_0^2}{L^2} \sqrt{\frac{N_l + 1}{N + 1}}, \tag{2}$$

$$b = \frac{0.0539}{\beta B} \times (1 + \cos^2 \theta)^{\frac{3}{4}} \times \frac{(1 + 0.038 \ln \frac{L_{tr}}{X_0})}{\sqrt{L X_0 \sin \theta}}. \tag{3}$$

In above formulae, N_l is the number of DC sensitive layers, N —the number of tracker hits, $a_0 = 2.12 \times 10^{-3} c / \text{GeV}$, L_0 —the DC thickness as difference between its outer and inner radii, L —distance passed by a particle inside the DC, L_{tr} —track length in the DC (all distances in meters), β —particle velocity normalized to the speed of light, B —magnetic field in tesla, θ —particle polar angle, X_0 —average radiation length of wires and He : C₃ H₈ = 6 : 4 gas mixture over the DC volume ($X_0 = 187$ m). Parameters L , L_0 and θ are illustrated in the Fig. 3. The number N of hits is calculated as the number of layers crossed by a particle. If a particle makes more than one full revolution, only first revolution hits are counted. If a particle produces less than 7 DC hits, its track is considered to be not reconstructed due to lack of information.

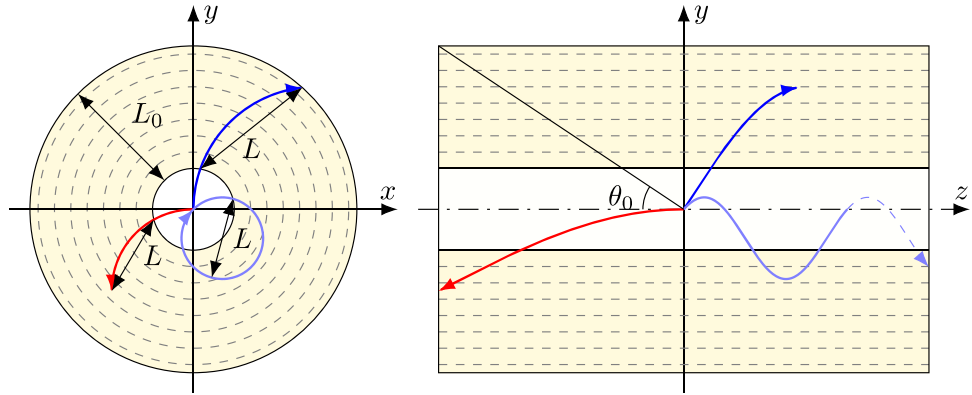
The polar angle DC resolution σ_{θ} is defined as a quadratic sum of multi-scattering component σ_{θ}^{MS} and spatial resolution σ_{θ}^0 :

$$\sigma_{\theta}^{MS} = \frac{0.014}{\beta p} \sqrt{\frac{L_{tr}}{X_0}} \left(1 + 0.038 \ln \frac{L_{tr}}{X_0} \right), \tag{4}$$

$$\sigma_{\theta}^0 = \begin{cases} 1.281 \times 10^{-3} / \sqrt{N_z}, & \theta \leq \theta_0 \\ 3.08 \times 10^{-3} \sin^2 \theta / \sqrt{N_z}, & \theta > \theta_0 \end{cases}, \tag{5}$$

where p —momentum in GeV / c, N_z —the number of z-coordinate measurements by stereo layers, and $\theta_0 = 40.16^\circ$ corresponds to the polar angle of the DC outer edge (see Fig. 3). Full momentum p resolution is defined as

Fig. 3 Track geometry parameters



$$\sigma_p = p \sqrt{a^2 p_{\perp}^2 + b^2 + \cot^2 \theta \times \sigma_{\theta}^2}, \tag{6}$$

where resolution coefficients a and b come from equations 2 and 3 correspondingly. The resulting simulated momentum resolution is shown in Fig. 4.

In addition to momentum measurement both DC variants could provide two particle identification options: dE/dx measurement and cluster counting.

The mean value of specific ionization loss is calculated using modified Bethe-Bloch equation tuned to BaBar experimental data [18] of truncated mean dE/dx dependence on β and γ .

$$BB(\beta, \gamma) = \frac{22.88}{\beta^{2.012}} \left(17.99 - \beta^{2.012} - 0.2906 \ln \left(\frac{1 + 3.655 \times 10^{-19} (\beta\gamma)^{8.513}}{1 + 0.2848 (\beta\gamma)^{8.513}} \right) \right). \tag{7}$$

The dE/dx resolution is described by an empirical BaBar equation [18]

$$\frac{\sigma_{dE/dx}}{\langle dE/dx \rangle} = 0.05 \left[\frac{N_{hot}}{N_0} \right]^{-0.6594} \left[\frac{L_{tr}}{L_0} \right]^{-0.2844} \times (1 + 0.01054(x - 5.632)^2) \times (1 + 0.007135(p_{\perp} - 4.141)^2), \tag{8}$$

where $N_0 = 40$, $L_0 = 100$, N_{hot} is defined as the number of active hits on a track, L_{tr} —track length in cm, p_{\perp} —transverse momentum in GeV / c and $x = BB(\beta, \gamma) / BB_{min}(\beta, \gamma) - 1$. Simulated dE/dx is shown in Fig. 5.

The number N_{cl} of ionization clusters is generated by Poisson distribution with the mean value

$$\lambda = \frac{dE/dx}{dE/dx_{min}} L_{tr} \delta_{cl}, \tag{9}$$

where δ_{cl} is the expected specific number of ionization clusters for a minimum ionizing particle. Then N_{cl} is normalized

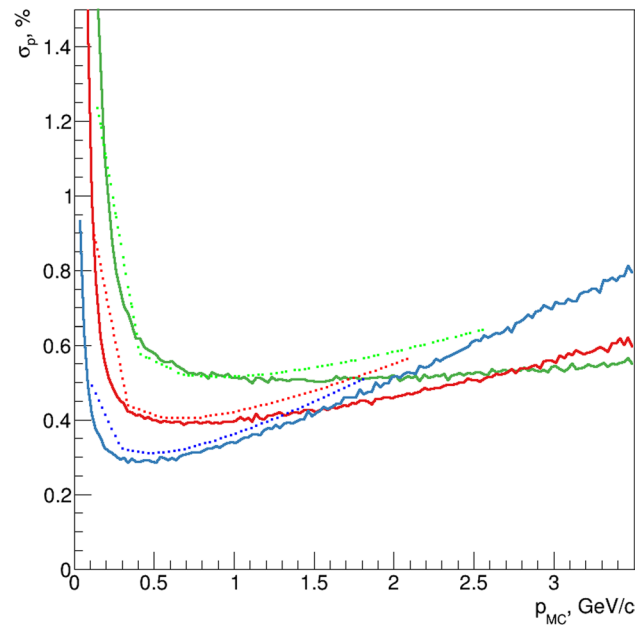


Fig. 4 Momentum resolution as a function of momentum depending on polar angle for simulated pions. Blue, red and green lines—results for tracks with $\theta = 90^\circ, 60^\circ$ and 45° . Solid lines—fast simulation; dotted lines—SCT chamber standalone simulation [17]

to L_{tr} to obtain the specific number of clusters dN_{cl} / dx . An example of dN_{cl} / dx for $\delta_{cl} = 12.5 / \text{cm}$ corresponding to the “non-classical” DC option He : $iC_4 H_{10} = 9 : 1$ gas mixture (see [19]) is shown in Fig. 6.

Likelihood

The tracker provides two sets of likelihoods L , one for dE/dx and one for dN_{cl} / dx . Hypothesis of measured track kind h is one of e, μ, π, K , or proton for each set. Specific energy loss is described by $L(h; p, dE/dx)$, ionization cluster density by $L(h; p, dN_{cl} / dx)$.

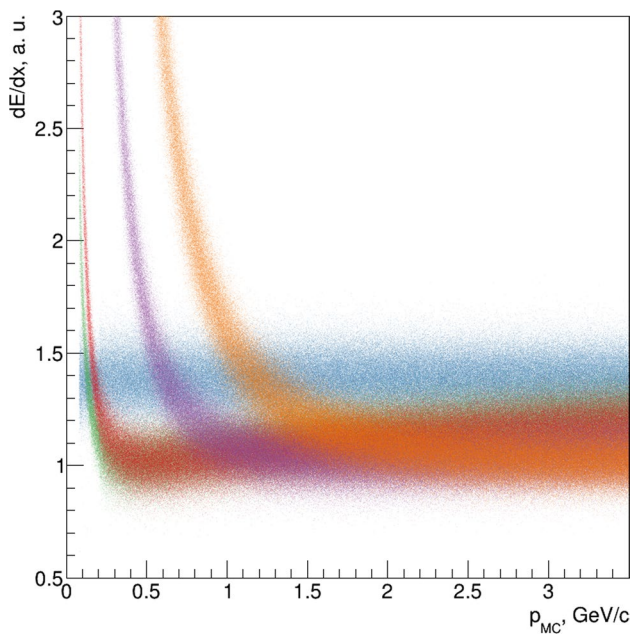


Fig. 5 dE/dx vs MC particle momentum: μ (green), π (red), K (violet) and p (orange)

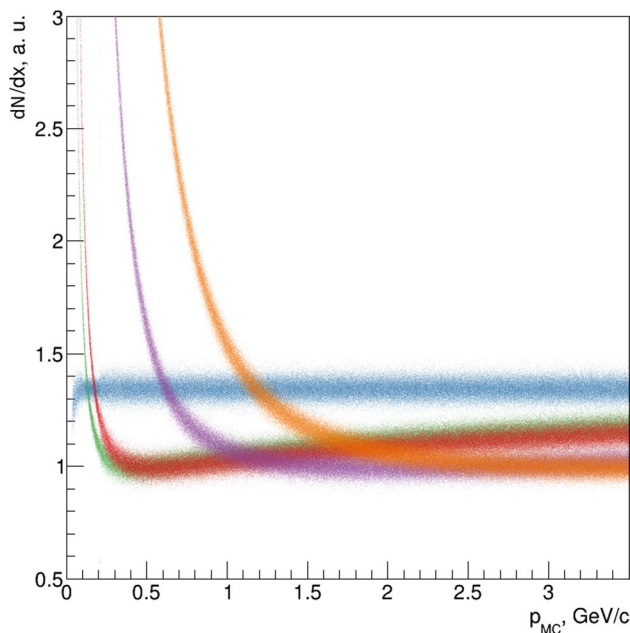


Fig. 6 dN_{cl}/dx vs MC particle momentum: μ (green), π (red), K (violet) and p (orange)

Output

The tracker response contains measured particle momentum, specific ionization loss and number of ionization clusters,

and corresponding likelihoods. Momentum \mathbf{p} is calculated in the point of closest approach of track helix to the z -axis.

FARICH

The FARICH option is well studied, enabling use of stand-alone full simulation based on beam test results with FARICH module prototype [20].

The calculation of FARICH subsystem response begins with emulation of the expected number $N_{ph.e.,0}$ of detected photoelectrons as a function of the impact angle in ρ - z plane and velocity. The function is based on the full simulation study and includes not only the actual Cherenkov photons contribution, but also electronic noise effects. The parameter $N_{ph.e.}$ is generated from a Poisson distribution around parameter $N_{ph.e.,0}$. If $N_{ph.e.}$ is less than 4, then it is assumed that the corresponding Cherenkov ring is not reconstructed, and velocity can not be determined. Otherwise, for $N_{ph.e.} \geq 4$, the ring is reconstructed. The generated normalized velocity β is smeared by Gaussian distribution with standard deviation taken from results of the full simulation. The dependence of $N_{ph.e.}$ and β on incident particle momentum is shown in Fig. 7.

Likelihood

FARICH provides up to two measurements per one track: $N_{ph.e.}$ and/or β . When only $N_{ph.e.}$ is measured, the likelihood is $L(h) = L(h; p, N_{ph.e.})$, where h is the particle type hypothesis. When both β and $N_{ph.e.}$ are available, $L = L(h; p, N_{ph.e.}) \times L(h; p, \beta)$.

Output

FARICH simulation yields number of expected $N_{ph.e.,0}$ and registered $N_{ph.e.}$ photoelectrons, measured β and its error.

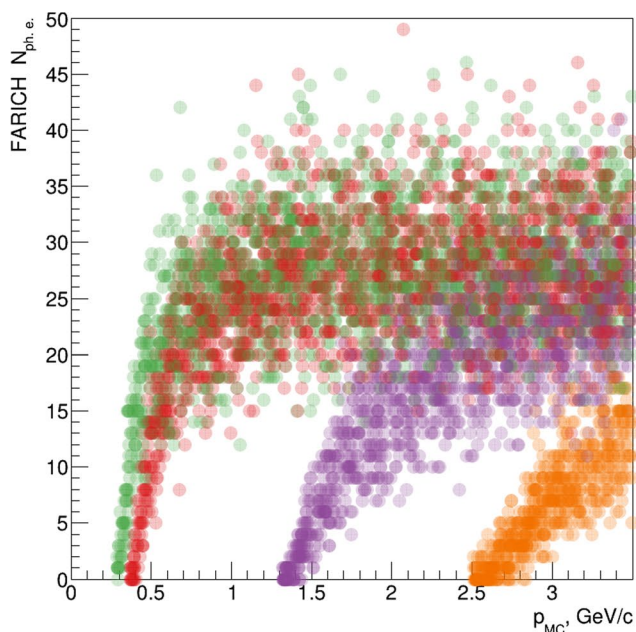
Calorimeter

The calorimeter is based on pure CsI scintillating crystals of approximately 33 cm \times 6 cm \times 6 cm in size. Its characteristics are studied with test beams [21] and stand-alone simulations [22].

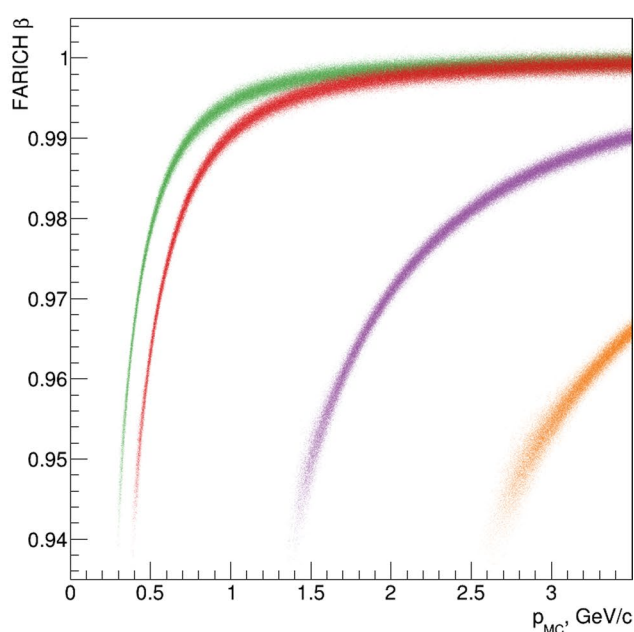
Energy Resolution

The calorimeter energy resolution σ_E is described by the sum in quadrature

$$\frac{\sigma_E}{E} = \sigma_0 \oplus \frac{\sigma_4}{\sqrt[4]{E}} \oplus \frac{\sigma_2}{\sqrt{E}} \oplus \frac{\sigma_1}{E}, \tag{10}$$



(a) The number $N_{\text{ph. e.}}$ of detected photoelectrons vs p_{MC} .



(b) The reconstructed β vs p_{MC} .

Fig. 7 FARICH response to different particles kinds: μ (green), π (red), K (violet) and p (brown)

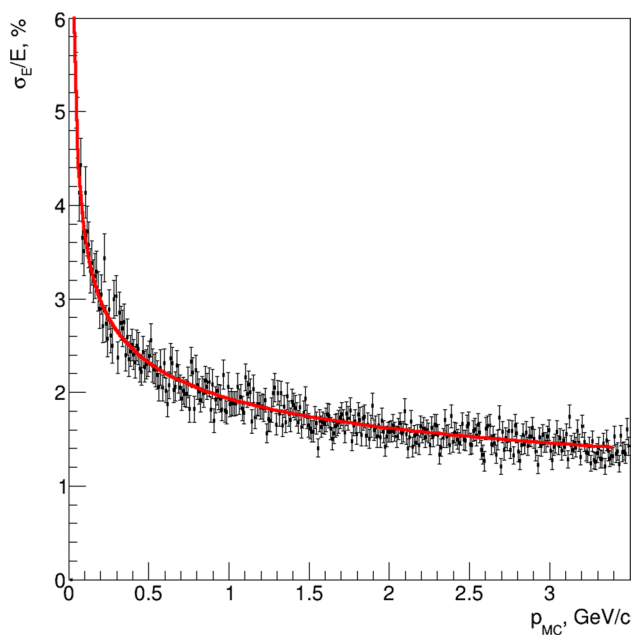


Fig. 8 Calorimeter energy resolution (points) and experimental result from [21] (line)

where the term σ_4 corresponds to the fluctuation of electromagnetic shower leakage, σ_2 corresponds to the statistics of photoelectrons, and σ_1 represents electronic noises. The current prototype gives the constant term $\sigma_0 = 0$, $\sigma_4 = 1.9\%$, $\sigma_2 = 0.33\%$ and $\sigma_1 = 0.11\%$ (see [21]). The obtained energy resolution dependence on photon energy is shown in Fig. 8.

Cluster Size

The size of a cluster is characterized by its radius. Photons and e^\pm produce electromagnetic showers with the cluster radius of 12 cm, which corresponds to 3 Molière radii of CsI $R_M = 3.57$ cm or 4×4 crystals, while for minimally ionizing particles 6 cm is taken to cover about 2×2 crystals.

Nuclear interactions of hadrons in the calorimeter are neglected.

Angular Resolution

The particle entrance point (r, θ, φ) to the calorimeter is used to reconstruct the cluster position (r', θ', φ') , where the azimuthal and polar angles are smeared by resolution function

corresponding to Gaussian functions with mean equal to zero and standard deviations σ_θ and σ_ϕ correspondingly. The parameters σ_θ and σ_ϕ depend on energy and θ of a particle, with dependence obtained from Geant4 simulation of the calorimeter [22]. Figure 9 presents simulated azimuthal angle resolution.

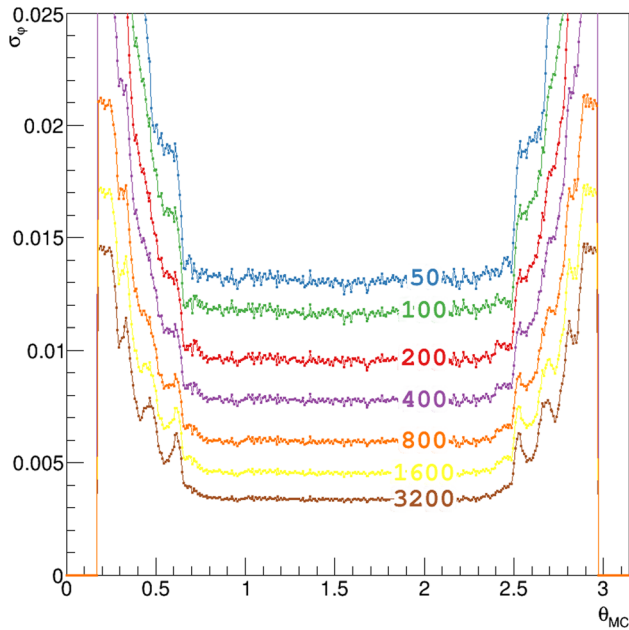


Fig. 9 Calorimeter azimuth angular resolution: different series corresponds to energies expressed in MeV at the plot

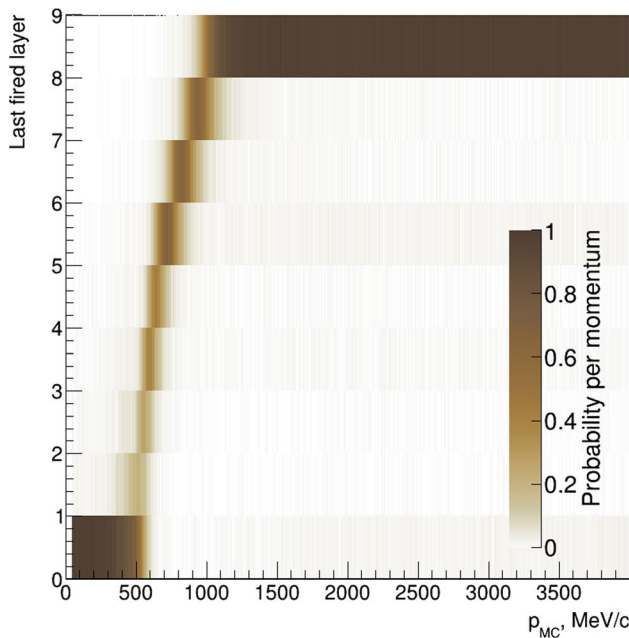
Calorimeter information is used to calculate neutral particle momentum.

Muon System

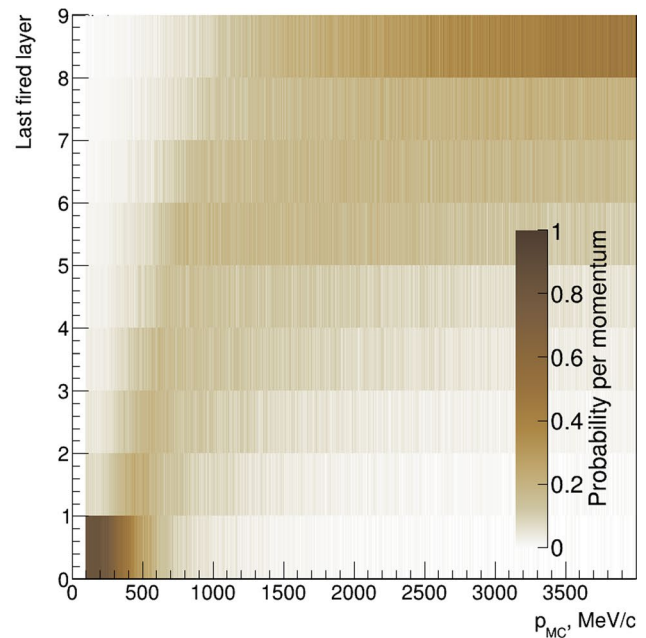
The muon system tool relies on results of the full Geant4 simulation of the detector produced with Aurora. Multidimensional histograms with the system response for muons and charged pions were prepared as input to the fast simulation. An illustration of a single muon event with muon system elements being hit is shown in Fig. 1. The phase space of total particle momentum (index i) and polar angle (index j) is divided into bins A_{ijl} . Index l corresponds to the most outer muon system layer with energy deposition more than 1 MeV (no requirements on time applied). If a particle does not produce any significant hits in the muon system, l is set to zero. In that way each region of p - θ space has an associated one-dimensional l -histogram with 9 bins (see Fig. 10), which is used to generate the muon system output in the fast simulation. For all particles, except muons and charged pions, the muon system response is set to zero at the moment.

Likelihood

The likelihood $L(l; p, \theta)$ for μ and π is determined from the response distribution histograms described above. For other hypothesis, namely electron, kaon and proton, L is set to 1, if there is no signal in the muon system, otherwise $L = 0$.



(a) μ^+



(b) π^+

Fig. 10 The last fired muon-system layer depending on a particle momentum, for particles with polar angle $\theta = \pi/3$

Event Reconstruction

When all particles are processed by detector subsystems tools, the reconstruction algorithm merges information from calorimeter and tracking system according to the following:

- Geometrically overlapping calorimeter clusters are merged, and their parameters, such as energy, time, coordinate, and size are recalculated. This way a pool of non-overlapping clusters is formed.
- Each reconstructed track is prolonged to the calorimeter. If the track crosses a cluster from the pool, the cluster becomes associated with the track and removed from the pool.
- All calorimeter clusters not attached to tracks are interpreted as neutral.

Particle Identification

The fast simulation provides a set of standard classifiers to distinguish between different types of charged particles: e^\pm likeness, μ/π , π/K and K/p separation. All numbers lay in the range $[0, 1]$. For each subsystem s we form a pair of likelihoods L_i and L_j — probability to obtain response r_s for measured momentum \mathbf{p} —for two hypotheses H_i and H_j . Then we can calculate how much H_i is preferred to H_j :

$$F_{ij}(\mathbf{p}) = \frac{\prod_s L_i(r_s, \mathbf{p})}{\prod_s L_i(r_s, \mathbf{p}) + \prod_s L_j(r_s, \mathbf{p})}. \tag{11}$$

F is monotonically transformed likelihood ratio $R = L_j/L_i$: $F = 1/(1 + R)$, and it can be interpreted as normalized likelihood ratio or likelihood fraction.

An example of likelihoods ratios F for μ/π and π/K hypothesis, using dE/dx and FARICH information at $p_{MC} = 1.6\text{GeV}/c$, is shown in Fig. 11.

Results and Examples

Here we demonstrate several tasks where the fast simulation package would be useful and how it can be used within Aurora framework.

Performance

The fast simulation package performance is compared to the full simulation. In the Aurora release 2.0.0 the full simulation uses the Geant4 version 10.07.p03, includes at least basic geometry description for each detector

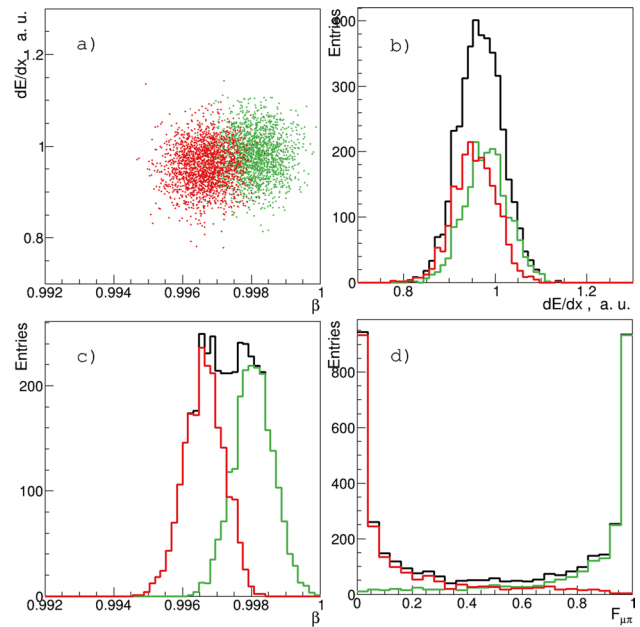


Fig. 11 The relative likelihood $F_{\mu\pi}$ (see eq. 11) (d) constructed by combining the FARICH (c) and dE/dx (b) information with the track momentum $p_{MC} = 1.6\text{GeV}/c$. (a) Shows correlation of β and dE/dx

Table 1 Simulation performance: mean time t spent per event and its RMS, mean initialization time t_{init} and its RMS, obtained with inclusive J/ψ events

	t	RMS (t)	t_{init}	RMS (t_{init})
Full	84 ms	113 ms	10.2 s	0.9 ms
Fast	0.59 ms	2.35 ms	109 μs	14 μs

subsystem, and is expected to consume up to about two times more computing resources in the final variant. Test samples of ten thousand inclusive J/ψ events are used to measure the performance. Mean spent time t per event and dispersion of t , as well as algorithm initialization time t_{init} with its dispersion are summarized in Table 1. Currently, the fast simulation requires ~ 150 times less time per event than the full simulation. One should also keep in mind that this comparison does not account for digitization and reconstruction stages mandatory in the full simulation chain analysis.

Particle Separation Power

Using the fast simulation one can study how performance of different subsystems affect the particle separation power. These studies have been performed with the previous version of simulation software, and the results

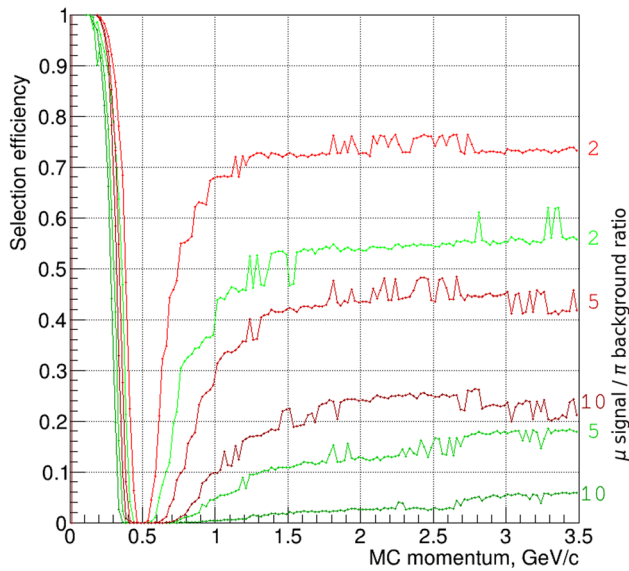


Fig. 12 Muon selection efficiency for several μ -signal to π -background rates (shown near the lines). Red lines represents dN_{cl}/dx , while greens— dE/dx

are previously published [23, 24]. For instance, primary muons and pions were generated with momentum up to 3.5 GeV/c with polar angle $\theta = 90^\circ$. We use $F_{dE/dx}$ and $F_{dN_{cl}/dx}$ likelihoods ratios to estimate a selection efficiency dependence on initial momentum keeping signal/background ratio fixed to 2, 5, and 10, and assuming the initial number of both event types to be equal. The comparison of dE/dx and dN_{cl}/dx options is shown in Fig. 12.

Overlapping Clusters in the Calorimeter

Cluster overlapping in the calorimeter leads to inefficiency of particle reconstruction. The effect is demonstrated with $e^+e^- \rightarrow \pi^0\gamma$ events with $\pi^0 \rightarrow \gamma\gamma$. The efficiency $\epsilon_{3\gamma}$ of all three photon reconstruction is studied as a function of center of mass energy \sqrt{s} and radius of electromagnetic cluster. The later can be changed through the following line in configuration file:

```
1 sct_alg.CaloSystemTool.  
   caloClSizeEGamma = 0.05 * units.m
```

The result is shown in Fig. 13. The efficiency $\epsilon_{3\gamma}$ is limited by the calorimeter geometrical acceptance.

The peak detector occupancy is expected to be about 300 kHz at J/ψ resonance. Issues associated with overlapping clusters and calorimeter showers shape are obviously important and will be addressed in future work.

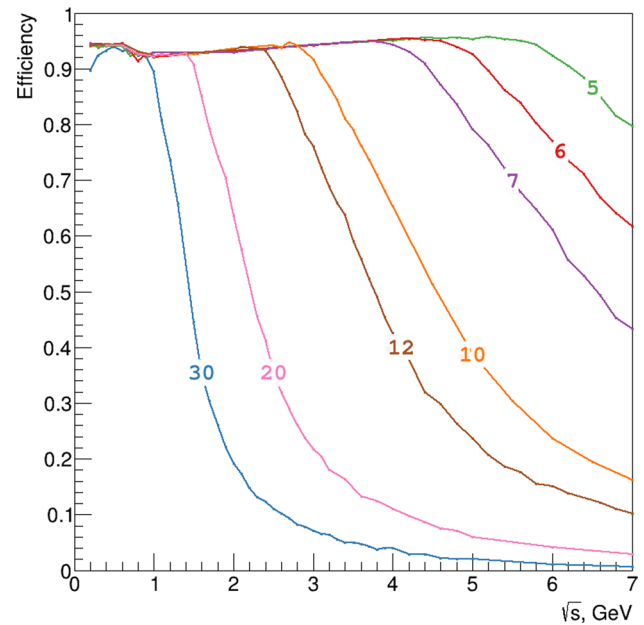


Fig. 13 3 photon reconstruction efficiency $\epsilon_{3\gamma}$ in process $e^+e^- \rightarrow \pi^0\gamma \rightarrow 3\gamma$ for different EM-shower cluster sizes (shown on the plot in cm)

J/ψ Two-Photon Invariant Mass Spectrum

The invariant mass of two photons $M_{inv}(\gamma\gamma)$ is investigated using inclusive J/ψ decays to study the expected kinematic spectra (Fig. 14). Two prominent peaks, corresponding to

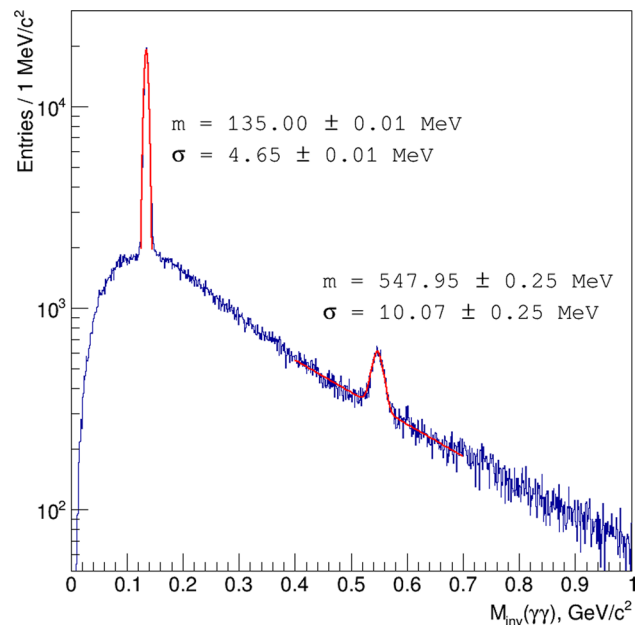


Fig. 14 Invariant masses of two photons in decays of J/ψ . Red lines show fit of π^0 and η mesons peaks

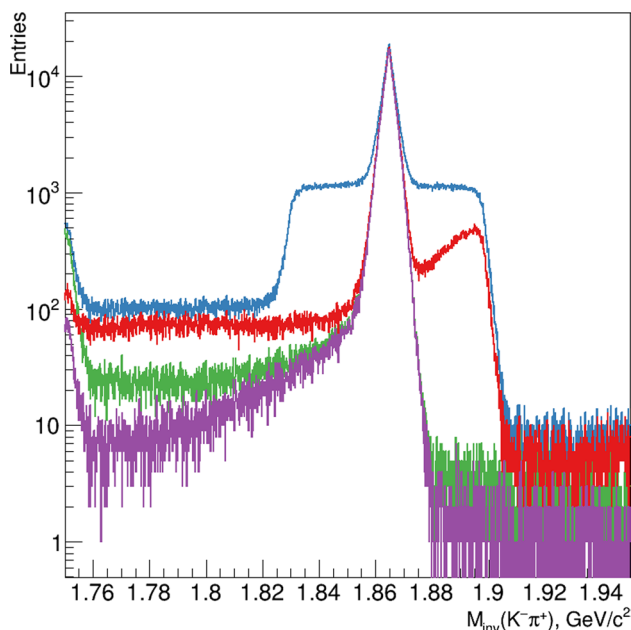


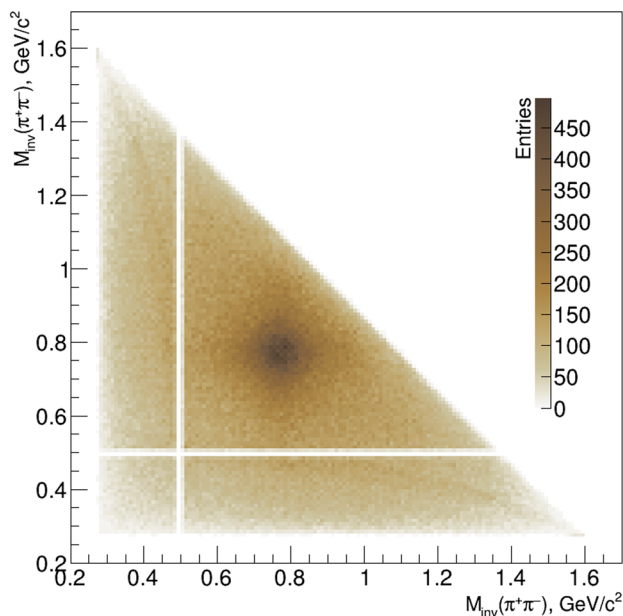
Fig. 15 Reconstruction $D^0 \rightarrow K^- \pi^+$ from inclusive decay of $\psi(3770)$. Blue line—no PID cuts, red— K cut, green— π cut, violet— K and π cuts

π^0 and η mesons, are visible. The upper half of the π^0 peak is approximated by Gaussian and the η peak with side bands by a sum of a Gaussian and exponential function to show the mass resolution.

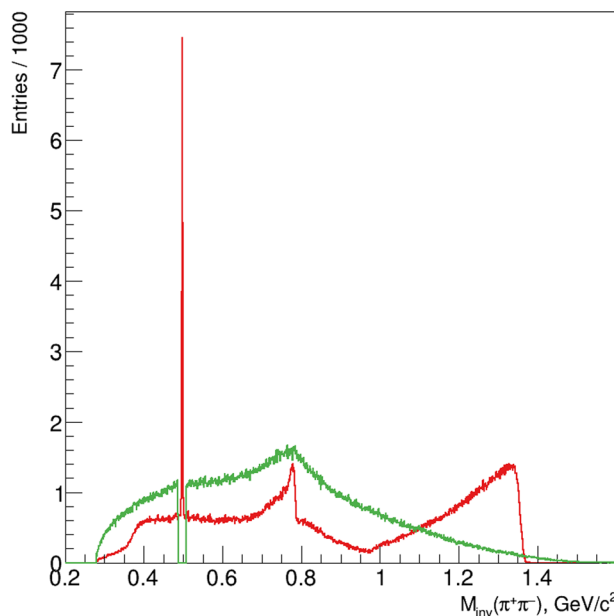
Reconstruction of D^0 Mesons from $\psi(3770)$ Decays

The decay $\psi(3770)$ to $D^0 \bar{D}^0$ is a good source of D -mesons pairs, with D -meson momentum around 287 MeV/ c at the lab frame. Here we demonstrate D^0 reconstruction in two final states $D^0 \rightarrow K^- \pi^+$ and $D^0 \rightarrow 2(\pi^+ \pi^-)$. The dataset of $\psi(3770)$ decays, which corresponds to one day of SCT operation, was generated using EvtGen [25] primary generator and passed through the fast simulation.

Using the analysis tool available in Aurora we reconstruct all pairs of $K^- \pi^+$ with and without limitations on $F_{K\pi} > 0.2$ and $F_{\mu\pi} < 0.8$ for pions, and $F_{K\pi} < 0.8$ for kaons. Obtained $K^- \pi^+$ invariant mass spectra with different selection criteria are presented in Fig. 15. It demonstrate how PID cuts help to



(a) $M_{inv}(\pi^+ \pi^-)$ vs another $\pi^+ \pi^-$ -pair $M_{inv}(\pi^+ \pi^-)$ distribution, when K_S^0 is forbidden.



(b) $M_{inv}(\pi^+ \pi^-)$ when another $M_{inv}(\pi^+ \pi^-)$ around the K_S^0 mass (red line) and when no K_S^0 is observed (green line).

Fig. 16 Reconstruction of $D^0 \rightarrow 2(\pi^+ \pi^-)$ from inclusive decay of $\psi(3770)$

purify the $D^0 \rightarrow K^- \pi^+$ signal, providing the detection efficiency about 85%.

The four charged pion final state of the D^0 meson is selected by invariant mass and by momentum magnitude for tracks with $F_{K\pi} < 0.8$ by applying $1.84 < M/(\text{GeV}/c^2) < 1.88$ and $0.27 < p/(\text{GeV}/c) < 0.3$. The $\pi^+ \pi^- \pi^+ \pi^-$ final state is resulted from Cabibbo-favoured decay $D^0 \rightarrow (K_S^0 \rightarrow \pi^+ \pi^-) \pi^+ \pi^-$ and single Cabibbo-suppressed decay $D^0 \rightarrow 2(\pi^+ \pi^-)$. The $K_S^0 \pi^+ \pi^-$ enriched sample is obtained requiring one $M_{\text{inv}}(\pi^+ \pi^-)$ to be around K_S^0 mass, while the Cabibbo-suppressed sample is produced forbidding $M_{\text{inv}}(\pi^+ \pi^-)$ be around K_S^0 mass and vetoing events with pions approaching closer than 1 mm to the beam crossing point. An internal dynamics of the decays $D^0 \rightarrow 2(\pi^+ \pi^-)$ and $D^0 \rightarrow K_S^0 \pi^+ \pi^-$ could be studied using distributions of $M_{\text{inv}}(\pi^+ \pi^-)$. Corresponding spectra are shown in Fig. 16. In states with K_S^0 one will easily see K_S^0 , $\rho^0(770)$, $\omega(782)$, $f_0(980)$ and $f_0(1370)$ resonance contributions, while K_S^0 -less state shows $\rho^0(770)$.

Conclusion and Outlook

In this paper we briefly describe the software environment of the SCT detector and formulate tasks arising before simulation. Some of these tasks are successfully solved with help of the fast simulation packages integrated into the SCT software framework. The internal logic of the fast simulation and package usage within the framework are shown. Main detector sensitive subsystems have been implemented relying on different detector response parameterization approaches. This implementation can be considered as a set of examples and templates for further package development, e.g. the introduction of an inner tracker [26] or FDIRC as a PID option [27]. Several examples of fast simulation application are provided to show opening possibilities of physical analysis and detector options studies.

Appendix A Code Example

The following part of Aurora job steering file illustrates how to create and tune the fast simulation object.

```

1 from Configurables import SctParSimAlg
2 import AuroraConditions as ACond
3
4 sct_alg = SctParSimAlg('SctAlg')#
5     Create a fast-sim detector.
6 sct_alg.RandomStreamName = "
7     fast_sim_random_seed"
8 # Load FARICH parametrization file
9     from the standard super c-tau
10    repository.
11 sct_alg.FARICHSystemTool.
12     parSimFarichFileName = ACond.
13     conditionFilePath('Simulation/
14     SctParSimTools', 'v01',
15     pi_ms_f1_mppc2_px3_d200_mla4_graph2d
16     .root')
17
18 # Load muon parametrization from the
19     standard file and from the local
20     file.
21 sct_alg.MuonSystemTool.
22     parSimMuonFileNameMu = ACond.
23     conditionFilePath('Simulation/
24     SctParSimTools', 'v01',
25     g4beamline_mu_plus_100k_parse.root
26     ')
27 sct_alg.MuonSystemTool.
28     parSimMuonFileNameMu = ACond.
29     conditionFilePath('/home/user_name
30     /run', '', './
31     fullG4_muon_system_mu.root')
32
33 # Set single value properties.
34 sct_alg.TrackSystemTool.trackMinPt =
35     0.010 * units.GeV
36 sct_alg.CaloSystemTool.
37     caloClSizeEGamma = 0.12 * units.m
38 sct_alg.CaloSystemTool.caloClSize =
39     3.57 * units.cm
40
41 # Set a two dimensional vector.
42 sct_alg.TrackSystemTool.trackLayerSt =
43     [ [5., 150.], [5., 160.], [5.,
44     180.], [5., 190.],
45     [6.473, 280.154], [6.747, 290.136],
46     [7.182, 310.863], [7.486,
47     321.938],
48     [6.603, 405.941], [6.799, 416.040],
49     [7.104, 436.741], [7.314,
50     447.606],
51     [6.741, 533.350], [6.895, 543.615],
52     [7.026, 554.088], [7.161,
53     564.762],
54     [6.778, 584.801], [6.919, 595.108],
55     [7.039, 605.606], [7.163,
56     616.289],
57     [6.746, 689.948], [6.865, 700.185],
58     [7.041, 720.090], [7.165, 730.775]
59     ]
60
61 # Set a vector property.
62 sct_alg.CaloSystemTool.caloResPar =
63     [0., .0011, .0133, .029]
64
65 sct_alg.OutputLevel=INFO# Set a
66     printing level.

```

Acknowledgements This work was financially supported by the Russian Science Foundation (Grant No 19-72-20114) and used the resources of the Siberian Supercomputer Center cluster (ICM & MG SB RAS, Novosibirsk).

Data availability The software described as well as data sets generated during the current study are available from the authors on reasonable request.

Open Access This article is licensed under a Creative Commons Attribution 4.0 International License, which permits use, sharing, adaptation, distribution and reproduction in any medium or format, as long as you give appropriate credit to the original author(s) and the source, provide a link to the Creative Commons licence, and indicate if changes were made. The images or other third party material in this article are included in the article's Creative Commons licence, unless indicated otherwise in a credit line to the material. If material is not included in the article's Creative Commons licence and your intended use is not permitted by statutory regulation or exceeds the permitted use, you will need to obtain permission directly from the copyright holder. To view a copy of this licence, visit <http://creativecommons.org/licenses/by/4.0/>.

References

- Bondar AE et al (2013) Project of a super Charm-Tau factory at the Budker Institute of Nuclear Physics in Novosibirsk. *Phys Atom Nucl* 76:1072–1085. <https://doi.org/10.1134/S1063778813090032>
- Epifanov DA (2020) Project of Super Charm-Tau Factory. *Phys Atom Nucl* 83(6):944–948. <https://doi.org/10.1134/S1063778820060137>
- Barnyakov AY (2020) The project of the Super Charm-Tau Factory in Novosibirsk. *J Phys Conf Ser* 1561(1):012004. <https://doi.org/10.1088/1742-6596/1561/1/012004>
- Belozorova M, Maksimov D, Razuvaev G, Sukharev A, Vorobyev V, Zhadan A, Zhadan D (2021) Software framework for the Super Charm-Tau factory detector project. *EPJ Web Conf.* 251(03):017. <https://doi.org/10.1051/epjconf/202125103017>
- Belozorova M, Maksimov D, Razuvaev G, Sukharev A, Vorobyev V, Zhadan A, Zhadan D (2021) in 9th International Conference on Distributed Computing and Grid Technologies in Science and Education, pp 375–380. <https://doi.org/10.54546/MLIT.2021.97.25.001>
- Kama S, Leggett C, Snyder S, Tsulaia V (2019) The ATLAS multithreaded offline framework. *EPJ Web Conf* 214(05):018. <https://doi.org/10.1051/epjconf/201921405018>
- Barrand G, Belyaev I, Binko P, Cattaneo M, Chytracsek R, Corti G, Frank M, Gracia G, Harvey J, van Herwijnen E, Maley P, Mato P, Probst S, Ranjard F (2001) GAUDI—a software architecture and framework for building HEP data processing applications. <https://gitlab.cern.ch/gaudi/Gaudi>
- YAML: YAML Ain't Markup Language. <https://yaml.org>
- Gaede F, Hegner B, Mato P (2017) PODIO: an event-data-model toolkit for high energy physics experiments. *J Phys Conf Ser* 898:072039
- Brun R, Rademakers F (1997) ROOT: an object oriented data analysis framework. *Nucl Instrum Method A* 389:81–86. [https://doi.org/10.1016/S0168-9002\(97\)00048-X](https://doi.org/10.1016/S0168-9002(97)00048-X)
- Agostinelli S et al (2003) Geant4—a simulation toolkit. *Nucl Instrum Methods Phys Res Sect A Accel Spectrom Detect Assoc Equip* 506(3):250–303. [https://doi.org/10.1016/S0168-9002\(03\)01368-8](https://doi.org/10.1016/S0168-9002(03)01368-8)
- Allison J et al (2006) Geant4 developments and applications. *IEEE Trans Nucl Sci* 53(1):270–278. <https://doi.org/10.1109/TNS.2006.869826>
- Allison J et al (2016) Recent developments in Geant4. *Nucl Instrum Method A* 835:186–225. <https://doi.org/10.1016/j.nima.2016.06.125>
- Bernet C (2018) Papas: a fast simulation of the particle flow. <https://indico.cern.ch/event/656491/contributions/2939165/>. FCC Week
- de Favereau J, Delaere C, Demin P, Giammanco A, Lemaître V, Mertens A, Selvaggi M (2014) DELPHES 3, a modular framework for fast simulation of a generic collider experiment. *JHEP* 02:057. [https://doi.org/10.1007/JHEP02\(2014\)057](https://doi.org/10.1007/JHEP02(2014)057)
- Shi XD, Zhou XR, Qin XS, Peng HP (2021) A fast simulation package for STCF detector. *JINST* 16(03):P03029. <https://doi.org/10.1088/1748-0221/16/03/P03029>
- Basok IY, Bedareva TV, Blinov VE, Grigoriev MD, Gusev GA, Kyshtymov DA, Prisekin VG, Todyshev KY (2021) The drift chamber project for the Super Charm-Tau Factory detector. *Nucl Instrum Method A* 1009(165):490. <https://doi.org/10.1016/j.nima.2021.165490>
- Todyshev K (2017) BaBar DCH dE/dx calibration and a new technique of energy loss calculation. BABAR Analysis Document #1698
- Grancagnolo F (2020) The evolution of drift chambers at e^+e^- colliders. <https://indico.inp.nsk.su/event/20/contributions/955/>. Instrumentation for Colliding Beam Physics
- Barnyakov AY, Barnyakov MY, Bobrovnikov V, Buzykaev A, Daniluyk A, Düren M, Hayrapetyan A, Katcin A, Kayan H, Kononov S, Kravchenko E, Kuyanov I, Ovtin I, Podgornov N, Pomuleva S, Schmidt M, Shalygin A, Traxler M (2022) Progress and perspectives of FARICH R & D for the Super Charm-Tau Factory project. *Nucl Instrum Methods Phys Res Sect A Accel Spectrom Detect Assoc Equip* 1039(167):044. <https://doi.org/10.1016/j.nima.2022.167044>
- Aihara H, Epifanov DA, Jin Y, Osipov AA, Prokhorova ES, Shwartz BA, Usov YV, Yudin YV (2019) Fast calorimeter on the pure CsI crystals for the modern e^+e^- super factories. *JPS Conf Proc* 27(012):010. <https://doi.org/10.7566/JPSCP.27.012010>
- Ivanov VL et al (2020) Simulation of the CsI crystal calorimeter of the detector of charm-tau factory in Novosibirsk. *JINST* 15(07):C07026. <https://doi.org/10.1088/1748-0221/15/07/C07026>
- Barnyakov AY et al (2020) Overview of PID options for experiments at the Super Charm-Tau Factory. *JINST* 15(04):C04032. <https://doi.org/10.1088/1748-0221/15/04/C04032>
- Barnyakov AY et al (2020) Particle identification system for the Super Charm-Tau Factory at Novosibirsk. *Nucl Instrum Method A* 958(162):352. <https://doi.org/10.1016/j.nima.2019.162352>
- Lange DJ (2001) The EvtGen particle decay simulation package. *Nucl Instrum Methods Phys Res Sect A Accel Spectrom Detect Assoc Equip* 462(1):152–155. [10.1016/S0168-9002\(01\)00089-4](https://doi.org/10.1016/S0168-9002(01)00089-4). www.sciencedirect.com/science/article/pii/S0168900201000894. BEAUTY2000, Proceedings of the 7th Int. Conf. on B-Physics at Hadron Machines
- Sokolov A, Maltsev T, Shekhtman L, Vadakepattu VK (2022) Development of compact TPC for future Super Charm-Tau Factory detector. *Nucl Instrum Meth A*. <https://doi.org/10.1016/j.nima.2022.167225>
- Schmidt M, Düren M, Hayrapetyan A, Barnyakov AY, Kononov SA (2020) DIRC options for the Super Charm Tau Factory. *JINST* 15(02):C02032. <https://doi.org/10.1088/1748-0221/15/02/C02032>

Publisher's Note Springer Nature remains neutral with regard to jurisdictional claims in published maps and institutional affiliations.